# Crystal-Arrested Phase Separation

Juan Sabin,* Arthur E. Bailey, Gabriel Espinosa,† and Barbara J. Frisken

*Department of Physics, Simon Fraser University, Burnaby, British Columbia, Canada V5A 1S6*

We have studied the interplay between phase separation and crystallization in a colloid-polymer mixture along one kinetic pathway in samples which exhibit three-phase equilibrium coexistence. In analogy with atomic systems, the range of the effective attractive interaction between colloids is sufficiently long to allow for a stable liquid phase. By direct imaging in microgravity on the International Space Station, we observe a unique structure, a ''crystal gel,'' that occurs when gas-liquid phase separation arrests due to crystallites within the liquid domain spanning the cell. From the initial onset of spinodal decomposition until arrest caused by this structure, the kinetics of phase separation remain largely unaffected by the formation of the third phase. This dynamic arrest appears to result from the stiffness of the crystalline strands exceeding the liquid-gas interfacial tension.

Mixtures of colloids and nonadsorbing polymers have been investigated extensively as a convenient model for a wide variety of fundamental properties of matter including phase behavior and phase transition kinetics [1,2]. The great flexibility of this system results from the tunable nature of the effective attractive interaction induced by the entropy of polymer added to a hard-sphere colloidal suspension. The dimensionless range of this interaction $\xi$ is defined as the ratio of the polymer's size to the colloidal particle size, and the strength of the interaction is set by the polymer concentration [3,4]. At a sufficiently long range of attraction, $\xi > 0.3$, the colloid-polymer (C-P) system exhibits a phase diagram including a region of triple coexistence of colloid-poor (gas), colloid-rich (liquid), and colloidal solid (crystal) phases [5]. In addition, the kinetics of phase separation in the region of coexistence of gas and liquid phases of the C-P samples are nearly identical to those of simple liquids or liquid mixtures with the colloid size determining the governing length scale [6]. These factors make the colloid-polymer mixture system a nearly ideal one in which to explore the kinetics of phase separation in the presence of three-phase coexistence.

Multiple routes to complete phase separation exist within the three-phase region but sedimentation limits observation of fundamental phenomena. Investigations of three-phase C-P phase separation have revealed a variety of kinetic pathways [7]. These kinetic regimes can be described in terms of the free-energy landscape of the system [8]. One pathway, in particular, referred to as regime $G$ [7], begins with gas-liquid phase separation followed by nucleation of crystals within the liquid phase. This occurs in the low- to mid-colloid volume fraction region of the three-phase triangle, centered between the underlying gas-liquid binodals. On Earth, gravity causes sedimentation of the crystals and stratification of the three phases. While gravity may not affect the early stages of this process, the later stages must surely evolve differently

without gravity. In this Letter, we report the detailed kinetics of this regime studied both on Earth and in microgravity on the International Space Station.

We prepared samples exhibiting three-phase coexistence at constant interaction range. Polymethylmethacrylate spheres, sterically stabilized by a thin surface layer of poly-12-hydroxystearic acid [9], were suspended in a 45:55 by mass mixture of decahydronaphthalene (decalin) and tetrahydronaphthalene (tetralin). This mixture nearly matches the refractive index of the colloidal particles and reduces van der Waals attraction. The polymethylmethacrylate particles were heat shocked to ensure equilibrium swelling caused by tetralin adsorption [10]. The colloidal particles were measured by static light scattering to have a 229 nm radius. Polystyrene, molecular weight $M_w = 13.2 \times 10^6$ g $\cdot$ mol$^{-1}$ and heterogeneity $M_w/M_n = 1.05$ (Polymer Laboratories Ltd., UK), was added to the solvent mixture, which is somewhat better than a theta solvent for polystyrene [1,11]. Static light scattering from the polymer in the solvent mixture measured a radius of gyration of 120 nm, yielding $\xi = 0.52$. The concentrations of the samples are shown in the phase diagram of Fig. 1.

On Earth, these samples show the kinetics described by Renth *et al.* for samples within regime $G$ [7]. After homogenization, taken as time $t = 0$, a rapid increase of the turbidity occurs, followed by formation of a diffuse interface between colloid-poor and colloid-rich phases. This interface sharpens and moves towards the bottom of the cell over time. The first crystals appear in the liquid phase within 6 hours and slowly settle forming a crystal phase in the bottom of the cell. No significant evolution of the samples occurs after 40 hours.

The colloid-polymer samples were studied in microgravity using the Binary Colloidal Alloy Test 5 instrumentation. The samples were sealed into glass cuvettes (Hellma) having a visible volume $4 \times 10 \times 20$ mm, and placed in a holder with optical-quality windows and
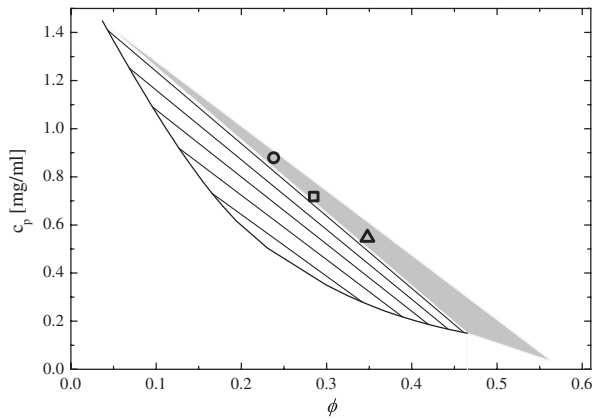
FIG. 1.   Schematic phase diagram of the C-P system graphed as polymer concentration $c_p$ vs colloid volume fraction $\phi$. The diagram is calculated from a mean-field analytic approximation [24]. The shaded triangle shows the three-phase coexistence region; the curve is the two-phase gas-liquid coexistence curve with several tie-lines shown. Samples 1 (open circle), 2 (open square), and 3 (open triangle), have $\phi = 0.24$, $0.29$, and $0.35$ and $c_p = 0.88$, $0.72$, and $0.55$ mg/mL, respectively.

launched via Space Shuttle to the International Space Station. Working one sample at a time, each sample was homogenized by repeatedly dragging a magnetic stir bar through it for about 20 min. Subsequently, the sample was imaged using a Kodak DCS760 camera with a Nikon AF-S Micro Nikkor 105 mm F2.8G macro lens and a Nikon SB-800 flash at regular intervals for several days. The flash provided transmission illumination of the sample at an angle ~60° relative to the camera lens. Each sequence of photographs was cropped, converted to grey scale and contrast enhanced using Adobe After Effects CS4 software [12].

The images show coarsening of phase separated domains until an arrest stops further evolution. Figure 2 shows a sequence of images taken of sample 2. The $t = 0$ image shows the sample just after mixing. A bicontinuous network of light and dark regions characteristic of spinodal decomposition becomes evident by 4 h. As the phases evolve, the domain size increases until approximately 20 h after mixing, when domain growth halts. Crystals are first visible approximately 7 h after mixing, similar to Earth-bound experiments, and subsequently additional crystals grow in the liquid phase throughout the sample. Crystal growth continues until the maximum crystallite size is comparable to the liquid domain size [13]. As seen in the time-lapse video of the sample [13], the crystals move and rotate prior to sample arrest but remain motionless after. The right end of the figure shows the arrested structure of each sample. This structure is quite stable; photographs of sample 2 taken one year after homogenization show the same characteristic domain size.

The characteristic length-scale $L$ of the phase separation process, representing the domain spacing, was determined by locating the nearest-neighbor peak in the azimuthally averaged 2D correlation function calculated from each image using a method previously described [6]. Evolution of $L$ is shown for all three samples in Fig. 3. All three samples show initial power law growth of $L$ with an exponent close to 1, characteristic of phase separation driven by minimization of the interfacial area. The final domain spacing for samples 2 and 3 is 1.2 mm, less than $1/3$ of the shortest dimension of the cuvette. Sample 1 shows a final domain spacing about 30% smaller than that of the other two samples.

The microgravity results agree with and extend Earth-bound measurements. Small-angle light scattering was
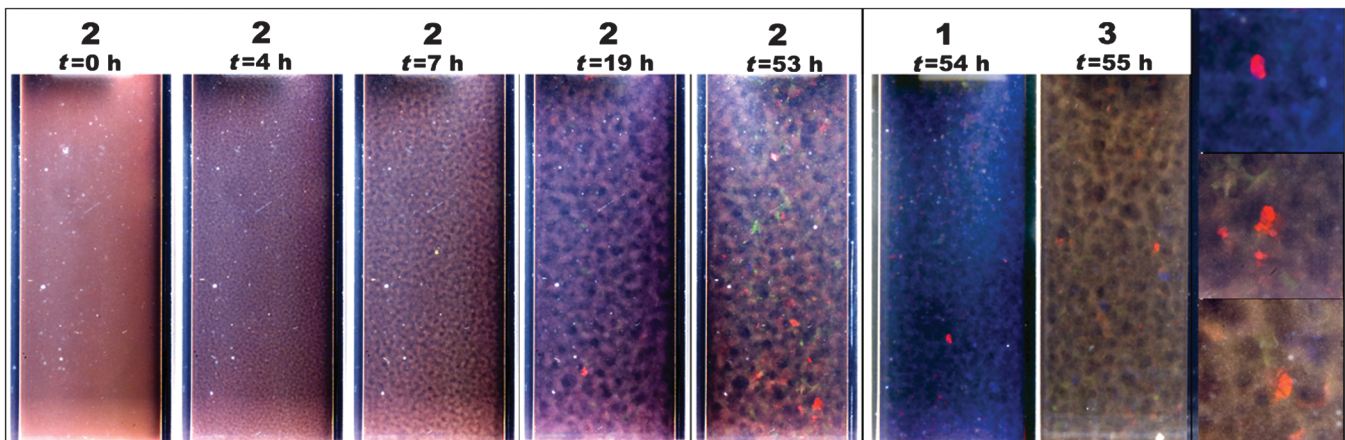


FIG. 2 (color).   Images of the samples in microgravity. The left five images show sample 2 evolving from time $t = 0$ to $t = 53$ h. Domains in the 19 and 53 h images have exactly the same pattern. Crystal visibility was improved in the 53 h image by an illumination change. The two images to the right show the other two samples at comparable times. Each of these seven images shows the full width of the cuvette. The three images on the far right show a 2.5 mm wide region of each sample with a prominent crystal: sample 1 at the top to sample 3 at the bottom. The crystal size is comparable to the liquid domain size.
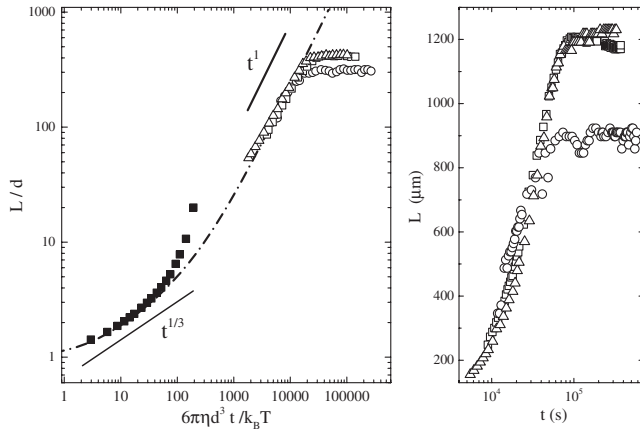
FIG. 3.  Time dependence of characteristic length scale for all
samples. The right-hand, semilog graph shows results from the
microgravity samples 1 (open circle), 2 (open square), and 3
(open triangle). The left-hand log-log graph shows the reduced
time vs reduced length scale for the microgravity samples and
scattering measurements (filled square) from a sample similar to
sample 2 in 1-g. The Furukawa function is shown with a dashed-
dotted line.

measured on Earth using a custom setup with an angular
range from 0.08 to 10 degrees [14]. Immediately after
homogenization, a scattering ring appears with a maximum
at a scattering wave vector $q_m = \frac{4\pi n}{\lambda} \sin(\theta_m/2)$, where $n$ is
the refractive index, $\lambda$ is the laser's wavelength, and $\theta_m$ is
the scattering angle at which the maximum intensity oc-
curs. This dominant wave vector is related to a character-
istic length scale of colloid concentration fluctuations by
$L \approx 2\pi/q_m$. After fitting a Gaussian function to a limited
number of points near the scattered peak to determine $q_m$,
the resulting $L$ data are graphed in Fig. 3. These results,
combined with microgravity results, are shown in the left
graph of Fig. 3 with time scaled by the characteristic time $\tau$
and $L$ by the colloid diameter $d$. The characteristic time is
given by $\tau = k_B T/(6\pi\eta d^3)$ where the viscosity $\eta$ was
estimated as that of the polymer-solvent mixture in the
free volume of each sample [6]. Scattering during the
initial stages of phase separation shows $L$ grows as $t^{1/3}$,
characteristic of diffusion-limited spinodal decomposition.
At intermediate times, the growth rate increases, consistent
with phase separation driven by minimization of the inter-
facial area [15]. At $t/\tau \sim 100$, gravity accelerates growth
as sedimentation severely increases the speed of coales-
cence. The microgravity image data, however, demonstrate
that without sedimentation $L$ continues to coarsen with a
growth law close to $t^1$. The combination of small-angle
light scattering and microgravity data agrees well with the
empirical expression proposed by Furukawa [16] for phase
separation of binary fluids (dashed line) until the phase
separation arrests. The same values of the adjustable pa-
rameters in this expression $A = 0.14$ and $B = 0.022$ were
used as resulted from experiments in binary liquids [16],
simple liquids [17], and the two phase region of a C-P

sample [6], and similar to the values found for polymer
blends [18]. The kinetics from the onset of spinodal de-
composition until nearly the time of arrest remain largely
unaffected by the formation of the third phase.

The novel final-state structure observed in microgravity
can be interpreted as a *cyrstal gel* where phase separation
arrests due to crystal growth resulting in a network of
crystals spanning the sample volume. This final state is
not the expected equilibrium state resulting from complete
phase separation in which we expect the three phases
to be fully separated and interfacial area minimized, likely
with either the liquid or crystal phases wetting the sample
cell [6]. We suggest that kinetic arrest results from the
crystalline deformation energy exceeding the surface ten-
sion energy so significantly that the probability of further
coarsening becomes exceedingly low. If sufficient crystal-
linity develops within the tubelike liquid domain, crystal
impingement and fusion will occur and the yield modulus
of the solid phase comes into play. Prior to this, the
gas-liquid interfacial tension could move the crystallites,
as observed in the time-lapse video, with viscous losses but
without an energy barrier.

The crystalline elastic energy can be compared to the
gas-liquid interfacial energy by considering a crystalline
cylinder with radius $r$ surrounded by a layer of colloidal
liquid of thickness $\Delta$. The total elastic energy for a tube of
crystallites with length $l$ at maximum elastic strain is $U_e = \pi r^2 l \delta_L^2 G_0/2$, where we take the maximum elastic strain as
the Lindemann parameter $\delta_L$ [19] and $G_0$ is the elastic
modulus of the crystal. Following an argument used for
hard-sphere colloids [19], we assume the elastic energy per
particle results from a dominant energy scale in the system
$\epsilon_g k_B T$, yielding the product $\delta_L^2 G_0 = (3\phi_c/16\pi a^3)\epsilon_g k_B T$.
Comparing the elastic energy with the total surface energy,
$2\pi l(r + \Delta)\epsilon_i \phi_l k_B T/a^2$ [20] where $\phi_l$ is the liquid-phase
colloid volume fraction and $\epsilon_i$ is the energy scale for
interfacial tension, we find that the surface energy exceeds
the elastic deformation energy when

$$\frac{\Delta}{r} > \frac{3}{64\pi}\left(\frac{\phi_c}{\phi_l}\right)\left(\frac{r}{a}\right)\left(\frac{\epsilon_g}{\epsilon_i}\right) - 1. \tag{1}$$

Since the colloid-polymer system has a single dominant
energy, the interaction energy, $\epsilon_g = \epsilon_i$. The values $\phi_l = 0.47$ and $\phi_c = 0.57$ result from the theoretical phase dia-
gram. From our images, we find typical crystal sizes
$2r \sim 350$ $\mu$m; thus, the liquid layer would need to be at
least 2200 $\mu$m thick to have sufficient surface energy to
exceed the elastic energy. This large value results from the
layer thickness scaling as the square of the crystal size and
from the large crystal size, $r/a \sim 750$, at the time of arrest.

This arrest mechanism likely applies only for samples
for which the kinetic path begins via spinodal decom-
position, generating a bicontinuous domain network, and
sufficient crystallinity is present. Without the bicontinuous
structure, crystalline strands cannot form a semirigid

structure spanning the sample. In the case of nucleated liquid droplets containing crystals, for example, the droplets would be free to coalesce, continually reducing surface energy without arrest. Even if a bicontinuous gas-liquid domain network forms, arrest will occur only if the crystalline strands form, thus, requiring a minimum crystallinity within the liquid-crystal domains. In fact, Eq. (1) for the relative thickness of the liquid layer has a critical value. For sufficiently small crystalline strands, an infinitesimal amount of liquid coating would be sufficient to overcome the yield modulus. From our approximation, the critical crystalline strand radius for our samples in units of the colloid size $r/a$ is ~55. Therefore, within the limitations of this simple model, crystalline strands smaller than approximately 110 colloids across cannot form a "crystal gel".

The smaller characteristic size at arrest in sample 1 results from earlier arrest of this sample compared to the others. This may result from the significantly smaller liquid phase volume in this sample as was observed on Earth and evidenced by sample 1's close proximity to the gas-solid boundary of the three-phase region. As domain coarsening proceeds, the initially liquid domain is simultaneously being partially consumed by crystallization. The arrest time is likely set by the shrinking liquid phase volume sufficiently confining the crystals causing crystalline strand formation, which occurs earlier in samples with a lower liquid to crystal phase volume ratio.

The arrest observed in this regime of the three-phase region is reminiscent of gelation of C-P mixtures at higher interaction strengths. Systems with a short range of attraction ($\xi < 0.2$) and intermediate interaction strengths and colloid concentrations gel via phase separation due to a metastable gas-liquid coexistence within the region of gas-crystal coexistence in the phase diagram [1]. Arrest occurs when the dense phase reaches a gelation boundary [21]. Systems with a longer range of attraction exhibit similar behavior, forming both stable [22] and unstable [23] gels. Gelation is expected at higher interaction potential because the strength of the interaction prevents rearrangement of the particles after contact, resulting in an amorphous non-equilibrium structure. In contrast, the arrest reported here occurs in a region where equilibrium is a three-phase state.

Experimentation in microgravity has revealed the fundamental behavior of this system. The kinetic pathway is confirmed but the small surface forces, which are overwhelmed in Earth's gravity, play a major role and lead to the formation of a unique crystal gel structure. The phases observed reach their final concentrations, but macroscopic phase separation is not achieved because the interfacial energy between the two lower-density phases is insufficient to overcome the stiffness of the crystalline strands. This effect may occur in any three-phase system whose interfacial and elastic energies result from a single dominant system energy scale. Further

investigation of other kinetic pathways may yield further insights into the details of phase separation in the presence of three phases.

*Present Address: Biophysics and Interfaces Group, Department of Applied Physics, University of Santiago de Compostela, E-15782 Santiago de Compostela, Spain.

†Present Address: Instituto de Física y Matemáticas, Universidad Michoacana de San Nicolás de Hidalgo, Edificio C3-B, Ciudad Universitaria, C.P. 58060, Morelia, Michoacán, Mexico.

[1] W. C. K. Poon, J. Phys. Condens. Matter **14**, R859 (2002).

[2] V. J. Anderson and H. N. W. Lekkerkerker, Nature (London) **416**, 811 (2002).

[3] A. Vrij, Pure Appl. Chem. **48**, 471 (1976).

[4] S. Asakura and F. Oosawa, J. Chem. Phys. **22**, 1255 (1954).

[5] H. N. W. Lekkerkerker, W. C. K. Poon, A. Stroobants, and P. B. Warren, Europhys. Lett. **20**, 559 (1992).

[6] A. E. Bailey, W. C. K. Poon, R. J. Christianson, A. B. Schofield, U. Gasser, V. Prasad, S. Manley, P. N. Segre, L. Cipelletti, W. V. Meyer, M. P. Doherty, S. Sankaran, A. L. Jankovsky, W. L. Shiley, J. P. Bowen, J. C. Eggers, C. Kurta, T. Lorik, Jr., P. N. Pusey, and D. A. Weitz, Phys. Rev. Lett. **99**, 205701 (2007).

[7] F. Renth, W. C. K. Poon, and R. M. L. Evans, Phys. Rev. E **64**, 031402 (2001).

[8] R. M. L. Evans, W. C. K. Poon, and F. Renth, Phys. Rev. E **64**, 031403 (2001).

[9] M. T. Elsesser and A. D. Hollingsworth, Langmuir **26**, 17 898 (2010).

[10] S.-E. Phan, W. B. Russel, Z. Cheng, J. Zhu, P. M. Chaikin, J. H. Dunsmuir, and R. H. Ottewill, Phys. Rev. E **54**, 6633 (1996).

[11] *Physical Properties of Polymers Handbook*, edited by J. E. Mark (Springer, New York, 2007), 2nd ed.

[12] P. J. Lu, *Gelation and Phase Separation of Attractive Colloids*, Ph.D. thesis, Harvard University, 2008.

[13] See Supplemental Material at http://link.aps.org/supplemental/10.1103/PhysRevLett.109.195701 for a time-lapse video of the evolution of sample 2. Note motion of crystals prior to arrest.

[14] D. Lee, I. A. Gutowski, A. E. Bailey, L. Rubatat, J. R. de Bruyn, and B. J. Frisken, Phys. Rev. E **83**, 031401 (2011).

[15] V. S. Nikolayev, D. Beysens, and P. Guenoun, Phys. Rev. Lett. **76**, 3144 (1996).

[16] P. Guenoun, R. Gastaud, F. Perrot, and D. Beysens, Phys. Rev. A **36**, 4876 (1987).

[17] Y. Garrabos, B. L. Neindre, P. Guenoun, B. Khalil, and D. Beysens, Europhys. Lett. **19**, 491 (1992).

[18] F. S. Bates and P. Wiltzius, J. Chem. Phys. **91**, 3258 (1989).

[19] Z. Cheng, J. Zhu, W. B. Russel, and P. M. Chaikin, Phys. Rev. Lett. **85**, 1460 (2000).

[20] E. H. A. de Hoog and H. N. W. Lekkerkerker, J. Phys. Chem. B **103**, 5274 (1999).

[21] W. C. K. Poon and M. D. Haw, Adv. Colloid Interface Sci. **73**, 71 (1997); P. J. Lu, E. Zaccarelli, F. Ciulla, A. B. Schofield, F. Sciortino, and D. A. Weitz, Nature (London) **453**, 499 (2008); E. Zaccarelli, P. J. Lu, F. Ciulla, D. A. Weitz, and F. Sciortino, J. Phys. Condens. Matter **20**, 494 242 (2008); T. Gibaud and P. Schurtenberger, J. Phys. Condens. Matter **21**, 322 201 (2009); F. Cardinaux, T. Gibaud, A. Stradner, and P. Schurtenberger, Phys. Rev. Lett. **99**, 118 301 (2007).

[22] J. C. Conrad, H. M. Wyss, V. Trappe, S. Manley, K. Miyazaki, L. J. Kaufman, A. B. Schofield, D. R. Reichman, and D. A. Weitz, J. Rheol. **54**, 421 (2010).

[23] L. J. Teece, M. A. Faers, and P. Bartlett, Soft Matter **7**, 1341 (2011).

[24] G. J. Fleer and R. Tuinier, Adv. Colloid Interface Sci. **143**, 1 (2008).